

Humans as Path-Finders for Safe Navigation

A. Antonucci, P. Bevilacqua, S. Leonardi, L. Palopoli, D. Fontanelli

Abstract—One of the most important barriers toward a widespread use of mobile robots in unstructured and human populated work environments is the ability to plan a safe path. In this paper, we propose to delegate this activity to a human operator that walks in front of the robot marking with her/his footsteps the path to be followed. The implementation of this approach requires a high degree of robustness in locating the specific person to be followed (the *leader*). We propose a three phase approach to fulfil this goal: 1. identification and tracking of the person in the image space, 2. sensor fusion between camera data and laser sensors, 3. point interpolation with continuous curvature curves. The approach is described in the paper and extensively validated with experimental results.

I. INTRODUCTION

When an autonomous mobile robot of remarkable size and mass navigates the treacherous waters of unstructured and human-populated environment, safety concerns and regulation constraints take centre stage and become a barrier for the adoption of this technology. To mitigate this problem, we advocate a mixed approach. When the mobile robot travels across a safe or segregated area, it can move in full autonomy, whilst whenever it enters a shared or dangerous area, the responsibility of the most critical decisions (i.e., motion planning) is shifted to a human operator.

Our reference scenario can be described as follows. The mobile robot starts its mission with a person standing in front. The robot looks at the person with its visual devices, extracts a number of important features and elects her/him as a leader. Then starts the second phase: the person walks to the destination, with the robot tracking its positions and following her/him moving along the path marked by her/his footsteps. After the leader reaches the destination, the path is memorised and can be used for future missions. Observe that *this is not* a standard leader-follower application in which the robot is allowed to sway sideways as far as it keeps a specified distance from its leader. In our case, the human is a path-finder and the robot follows her/his virtual footprints. The advantages are manifold. From the perspective of the robot, the human acts as an external module for the motion planning task, simplifying the complexity of the software components and of the sensing subsystems. From the perspective of the operator, he/she is in condition to drive a complex and heavy robot without any skill other than being able to walk. From the system integrator point of view, shifting the responsibility of motion planning to

a human whenever the robot moves in a difficult zone eases the pressure of regulation and safety constraints.

The idea outlined above can be seen as an original and modern application of the teach-by-showing approach to mobile robots moving in a complex and dynamic scenario. This is classified in the recent literature [1] as a very relevant and largely open problem and is the key methodological contribution made in this paper. Other contributions have a more technical nature and lie in the design of the system components. Our processing and execution pipeline has three phases: 1. identification of the leader within the front camera image frames, 2. fusion of the visual information with the information coming from other sensors, 3. reconstruction of a smooth and feasible path from the time series of the leader's positions, and controlled motion along the path.

The first phase is troublesome because the position of the leader is extracted from a noise source, in which an ambiguous classification of the different subjects in the scene is quite frequent. Our solution is to split the first phase in three sub-phases. The first one detects the objects of interest within the image using a state-of-the art convolutional neural networks (CNN) detector. The second sub-phase recognises the leader between the objects detected in the image. *The original solution of the paper* is to first train a neural network to classify the person and then use its last layer as a feature set. The feature identification is kick-started during the starting phase and is continuously refined during the system operation. The recognition properly said is performed by a K-Nearest Neighbour (KNN) classifier, which identifies the closest match with the leaders feature set between the objects identified in the frame. The third sub-phase consists of a tracking module, which ensures continuity in the estimated positions of the target across different frames.

In the second phase, we fuse the information on the leader position in the image with the measurements of a LIDAR sensor in order to reconstruct the correct location of the target and its headway distance from the robot. The resulting estimate is used as a refined and robust measurement in a multiple model Kalman filter (KF), which leverages two dynamic models for the prediction of human motions. The KF is used both to increase the robustness of the estimated positions and to track the target for some time even when he/she falls out of the visual cone (which is an unavoidable condition when the robot has to follow the reference footsteps in sharp turns). The filtered information is also fed back to the image tracking component to solve ambiguities and avoid misclassifications. The specific combination of tracking filter and neural network to estimate the position of the leader is *another important technical contribution of the paper*.

A. Antonucci, P. Bevilacqua, S. Leonardi, and L. Palopoli are with the Department of Information Engineering and Computer Science (DISI), University of Trento, Via Sommarive 5, Trento, Italy {alessandro.antonucci, luigi.palopoli}@unitn.it. D. Fontanelli is with the Department of Industrial Engineering (DII), University of Trento, Via Sommarive 5, Trento, Italy daniele.fontanelli@unitn.it.

The third phase processes the time series of the estimated position of the leader, refining the path and guiding the navigation. This step uses clothoid curves to interpolate the points, which produces a path with continuous curvature and easy to follow for a robot. Finally, the control module follows the estimated path and enforces the necessary safety policies.

The paper is organised as follows. In Section II, we summarise the most important existing results that we used as reference for this work. In Section III, we present our general architecture and provide details on the perception components that allow us to localise and track the leader. In Section IV, we show our solution for path reconstruction and the control strategy for following the path. The experiments supporting the validity of the approach are described in Section V. Finally, in Section VI we give our conclusions and announce future work directions.

II. RELATED WORK

People following is a complex activity requiring a combination of perception, planning, control, and interaction strategies. Following a specific person rather than any person adds more to the complexity of the problem and is largely classified as an open problem. The main issue is that in a complex scenario many people can look similar if they do not wear specific markers. Most of the methods developed in the last decade and surveyed by Islam et al [1], claim a good performance in detection and tracking of humans, while less of one half apply online learning or perform person re-identification, and even fewer do both. Target re-identification and recovery were handled first with probabilistic models (e.g. Kalman filters), features-based techniques and more recently with appearance-based deep networks, but these methods were not investigated further for human-following applications. The combination of detection, tracking, and recognition was proposed by Jiannig et al. [2] using the Speeded Up Robust Features (SURF). However, the key point matching did not show a sufficient level of robustness in our experimental tests with human figures. The complexity of the problem requires the combination of sophisticated learning approaches, model based filtering and path interpolation, as shown in this paper.

Object Detection. Object detection is in our framework the first element of the processing pipeline. For this component, we sought a good compromise between classification accuracy and achievable frame rate. The available methods range from object detection and segmentation methods [3], [4], [5], to specific solutions for human pose detection [6]. YOLO [4] is a very effective solution based on a single CNN; its main known disadvantage materialises when two classes have similar probabilities or the shape of the element is not perfect and the algorithm could produce different bounding boxes for the same object. Alternative solutions such as SSD [3] apply correction techniques to overcome the limitation [7]. After a thorough performance assessment, we evaluated that SSD was the best compromise for our application.

People recognition. People recognition in computer vision is difficult in its own right. An additional level of com-

plexity is introduced by the fact that the camera used for image acquisition is mobile. Traditional offline algorithms like Support Vector Machines (SVM) [8] are known to react quickly to classification queries, but are not a good fit for our scenario, because we lack a prior knowledge on who is going to be the leader and we need to be robust against possible changes in her/his appearance. Methods based on feature point matching [9] are known to be robust and are widely used to find small patterns in complex images, but in our tests the PRID450 (Person Re-IDentification) dataset [10] showed a high number of errors for low-res images and for deformable shapes such as humans clothes. Our final solution was based on the use of a K-Nearest Neighbours (KNN) classifier, which is an efficient training-free classification method. However, it requires the knowledge of representative points for the classification. For this information we used the last layer of a CNN, which gets trained with the different views of the leader. The idea of using a CNN classifier to extract the feature set was presented by Ristani et al. in [11], who proposed this idea to match detections from multiple cameras. The classifiers evaluated for this work are the Deep Neural Networks (DNNs) based GoogLeNet [12] and ResNet [13]. GoogLeNet showed the best performance in our experiments.

Person Tracking in the video frames. For person tracking, we could select from a large variety of approaches for the tracking of general objects (the fact that our object of interest is a person does not make a big difference in this case). Specifically, we considered: the Multiple Instance Learning (MIL) tracker [14], the Kernelised Correlation Filters (KCF) tracker [15], the Median Flow tracker [16], the Channel and Spatial Reliability Tracker (CSRT) [17], the Minimum Output Sum of Squared Error (MOSSE) tracker [18], the Generic Object Tracking Using Regression Networks (GOTURN) tracker [19], and the Tracking-Learning-Detection (TLD) [20]. After a thorough performance analysis, partly reported in Section V, we selected CSRT as the most suitable solution for our purposes.

Sensor fusion. Our application requires 3D reconstruction of the human pose. The combination between Stereo and RGB-D sensor with skeleton-based approaches proves very useful to this purpose and it is significantly simplified by the availability of public domain software components [21]. However, the simple use of visual information has known limitations such as the sensitivity to lighting conditions, and the high computation times. Laser-based sensors, on the other hand, are relatively reliable on a long range and are less computation hungry than vision based approaches. However, recognising a specific person from a slice of a 2D point cloud is hopeless. For this reason, moving along a direction frequently taken in robotics [22], [23], [24], we apply a combination of cameras and LIDARS. The use of separate systems for depth estimation and classification improves the robustness of the tracking system when one of the sensors fails; e.g., if the leader falls outside the camera field of view, we can still use the LIDAR sensor for some time assuming a certain degree of reliability of the specific-person following.

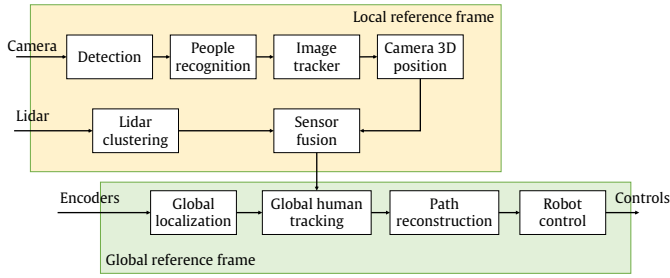


Fig. 1. Overall scheme of the algorithm.

III. TRACKING THE HUMAN PATH-FINDER

The proposed algorithmic framework is sketched in Figure 1. Before going into the details of the different building blocks, we succinctly describe the available sensing system and the model of the platform. The reference model for the robot is in this paper the unicycle, which can be described in discrete time by the following kinematic model:

$$s(t_{k+1}) = \begin{bmatrix} x_r(t_k) + \cos(\varphi_r(t_k))(t_{k+1} - t_k)v_r(t_k) \\ y_r(t_k) + \sin(\varphi_r(t_k))(t_{k+1} - t_k)v_r(t_k) \\ \varphi_r(t_k) + (t_{k+1} - t_k)\omega_r(t_k) \end{bmatrix} \quad (1)$$

where $s(t_k) = [x_r(t_k), y_r(t_k), \varphi_r(t_k)]^T$ is the state of the robot, the Cartesian coordinates $(x_r(t_k), y_r(t_k))$ refer to the mid-point of the rear wheels axle in the $X_w \times Y_w$ plane expressed in the $\langle W \rangle = \{X_w, Y_w, Z_w\}$ world reference frame, $\varphi_r(t_k)$ the longitudinal direction of the vehicle with respect to the X_w axis, $v_r(t_k)$ and $\omega_r(t_k)$ the longitudinal and angular velocities, respectively, and t_k the reference time instant, which is usually chosen an integer multiple of a fixed sampling time. Importantly, the proposed framework would be applicable to different robot dynamics; however, as explained next, the unicycle structure is particularly convenient for the class of applications we address.

Without loss of generality, we assume here that the choice of the sampling time $\delta_t = t_{k+1} - t_k$ is imposed by the sensor with the lowest sampling frequency. The assumed sensing configuration is based on the presence of rotation encoders on each of the rear wheels or any other sensing system able to provide ego-motion informations (e.g., IMUs, visual odometry). For the perception of the surroundings, the sensing system comprises a LIDAR and an RGB-D camera. The LIDAR data are used to both track human beings around the vehicle and to localise the vehicle inside the environment. The RGB-D camera is primarily used for the human detection and tracking. The laser scanner (an RPLidar A3¹) employed has a view of 360°, a maximum measuring distance up to 40 meters, and is typically operated at 20 revolutions per second. The RGB-D camera adopted is an Intel® RealSense™ D435², working in an ideal range spanning from 0.5 to 3 m, whose images are adopted in the vision-based detection and recognition system described in Section III-A.

¹<https://www.slamtec.com/en/Lidar/A3>

²<https://www.intelrealsense.com/depth-camera-d435/>

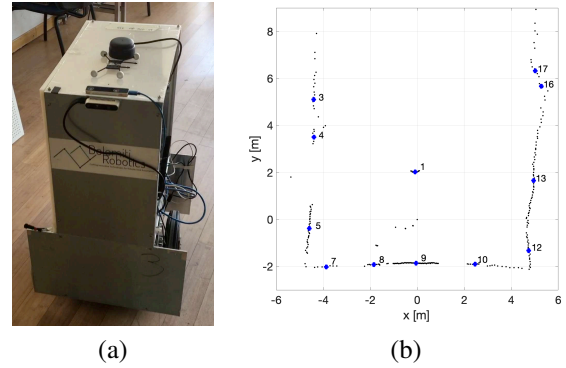


Fig. 2. (a) Robot sensing system setup, consisting of LIDAR sensor, RealSense D435, and RealSense T265 (for the visual odometry). (b) Laser scanned cloud points (thin black dots), with the object centroids (thick blue points) expressed in the LIDAR reference system $\langle L \rangle$.

The LIDAR and the camera are rigidly mounted on the top of the robot chassis (see Figure 2-a) and return the measurements in the reference frames $\langle L \rangle$ and $\langle C \rangle$, respectively, which are both rigidly linked to the robot (i.e., they operate with a local coordinates reference system). The transformation matrix ${}^L T_C$ between the two frames is estimated during the calibration phase in order to simplify sensor fusion.

A. Vision-based detection and recognition

The detection and recognition algorithm is almost entirely based on the images grabbed by the camera and comprises the detection, the recognition and image tracking phases. However, the information retrieved from the camera is interleaved with the one retrieved from the LIDAR (see Sec. III-B).

Detection: The vision-based detection module is used to periodically localize D people inside an image frame. Since we have chosen the latest version of YOLO available, YOLOv3 [25], and a lighter implementation of SDD, namely MobileNet [26] (designed to execute on low power devices), the detection module models the objects in view as the smallest bounding box that contains the detected element. In the starting phase, the person associated with the largest bounding box is recognised as leader.

Since the estimation drift affects all the tracking algorithms (and becomes particularly dangerous on long video sequences), we have assumed a proximity constraint along sequential frames. More precisely, during subsequent detection phases, if the detected target is too far away from the last known position of the leader, the detected shape is ignored and the information on the leader position is recovered from the LIDAR. The tolerance is expressed as a circle centred in the centroid of the last valid bounding box and whose radius is defined as

$$d = ts \left(\frac{w}{100} \right)^2, \quad (2)$$

where t is the time elapsed from the last correct detection of the leader, s is a tuning parameter empirically set as 0.05 and w is the width of the last bounding box from the image tracker, used to simulate the distance of the leader from the camera

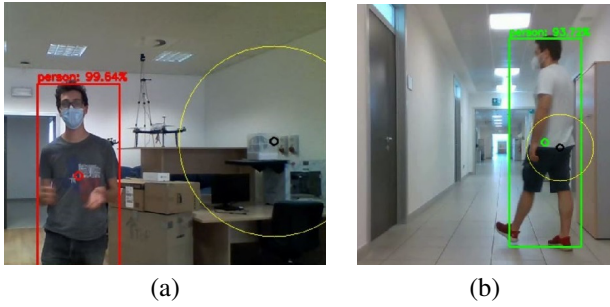


Fig. 3. Two examples of the application of the drift tolerance (2). In (a), the person is correctly classified as a mismatch because the bounding box is too far apart from the region defined by (2), while in (b) the leader is newly detected as expected.

and based on the fused information of Section III-B. Figure 3 shows an example where a person is immediately classified as a mismatch or a correct match.

People recognition: This module is used to understand if the found person corresponds to the leader or not, which enables a coherent connection between the detector and the tracker. Our method is based on a KNN algorithm. The KNN classifier uses images converted into points with DNN image classifiers: the ResNet50 [13], which produces a representation point in 2048 dimensions, and GoogLeNet [12] that produces a representation point in 1024 dimensions. If the leader is contained in the list of the D people found, the information is passed to the image tracker, otherwise the procedure loops the detection again.

As previously mentioned, the proposed recognition algorithm has a major distinctive feature: during the execution of the task, the generated representative points of the leader are fed back into the KNN. While this makes the leader recognition very robust in crowded spaces, a leader classified as a mismatch in the detection phase, cannot be re-evaluated as a valid leader and, hence, cannot be converted in a correct prediction. Albeit this unfortunate event may always happens in dynamic environments, the presence of the fusion algorithm in Section III-B mitigates its effects. Indeed, the results of the detection phase are fused with the LIDAR data before the information is fed into the neural network. However, if the estimation error of the human tracking filter in Section III-C exceeds the desired leader tracking uncertainty due to repetitive sensor or detection failures, the system reaches a faulty condition, the robot stops and the process should be reinitialised from scratch.

Image tracker: This module is periodically executed to track the leader location in a fixed number of m frames to avoid the problems generated due to long-term sequences. After that, the detection is performed again in order to strengthen the tracking performance. To this end, we implemented the methods that best fitted our requirements, i.e. KCF, CSRT and MOSSE. We emphasise that if a single detection fails or the leader is not found, the tracker cannot be started.

Overall detection and recognition algorithm: Since the image tracker pipeline performs an online learning classifica-

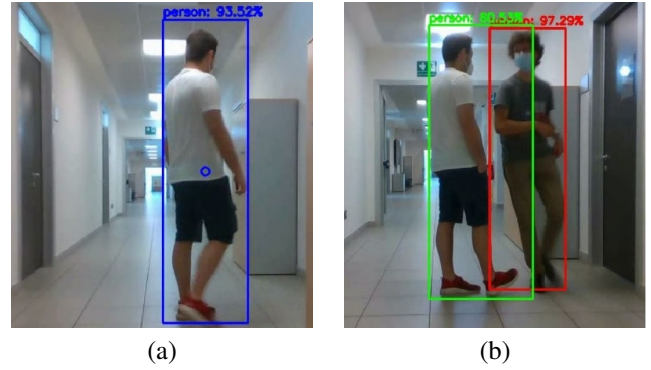


Fig. 4. (a) Initialisation phase: the detected leader is depicted with a blue rectangle. (b) Following phase: the leader is correctly recognised (green rectangle), while another person is a negative sample (red rectangle).

tion of the human, we start the pipeline with an *initialisation phase*, where only the detection module is working. This phase is designed in order to quickly train the KNN with a prior knowledge of the leader that will be enforced with the previously described feedback mechanism in the *robot following phase*. In the initialisation phase, which lasts for Δ_t seconds, the robot collects a series of bounding boxes used to create the set of positive representative points into the N -dimensional space of the KNN. Simultaneously, a negative sample is randomly picked up from a database and it is also given to the KNN to balance the number of positive and negative samples. The negative samples come from our customised version of the Market1501 dataset [27]. An example of the initialisation phase is shown in Figure 4-a. In the following phase, a first step of detection is carried out and all the found targets are checked with the drift-compensation threshold of (2). Then, the KNN classifier is used to distinguish between positive detections and negative ones (which are added to the negative dataset). In the successive m frames the image tracker is executed, and the result is passed to the fusion module. This workflow delivers a very high image processing performance and an improved robot localisation accuracy, as shown by the experimental data in Sec. V.

B. Local LIDAR-camera sensor fusion

The information coming from the vision-based algorithm are combined with the LIDAR in a local reference frame in order to make the procedure more robust, as aforementioned. An additional benefit of this phase is that the leader can be followed for some time also when he/she evades the vision cone of the RGB/D camera relying on the LIDAR information. The sensed data are fused in local coordinates, as explained next.

LIDAR clustering: Each scan delivered by the laser scanner provides a sequence of n measurement points in the form of $\mathcal{P} = \{p_1, \dots, p_n\}$, represented in polar coordinates as $p_i = (r_i, \alpha_i)$, i.e. a range and an angle expressed in the planar LIDAR reference frame $\langle L \rangle$, or in Cartesian coordinates, i.e. $p_i = (x_i, y_i) = (r_i \cos \alpha_i, r_i \sin \alpha_i)$ again in $\langle L \rangle$ (see Figure 2-b for an example of an actual scan). At time t_k , the mea-

sured points are filtered and grouped into m_k clusters based on the mutual Euclidean distances and on the richness, i.e. on a minimum number of sensed points for each cluster, each identified by the object centroid $o_j(t_k) = [x_j(t_k), y_j(t_k), 0]^T$, $j = 1, \dots, m_k$, and expressed in local coordinates, i.e. in $\langle L_k \rangle$.

Camera 3D position: The tracking module described in Section III-A returns a bounding box $[x, y, w, h]$ in the image frame, containing the (x, y) pixel coordinates of the top-left corner of the box, its width w and height h , which is then converted in the $\langle C \rangle = \{X_c, Y_c, Z_c\}$ pin-hole camera reference system. Notice that the depth information along the Z_c axis is retrieved via the RealSense™API. As a consequence, the centroid of the i -th bounding box $c_i(t_k) = [x_c(t_k), y_c(t_k), z_c(t_k)]^T$ can be expressed in the camera reference system $\langle C_k \rangle$ at time t_k .

Sensor fusion: Given the set of objects $\mathcal{O}_k = \{o_1(t_k), \dots, o_{m_k}(t_k)\}$ and the centroid(s) of the bounding box $c_j(t_k)$, taken at the same time instant t_k , we adopt a spatio-temporal correspondence algorithm with the two sets of measurements to decide if the tracked object is the same or a new one has entered into the scene. This simple algorithm, which adds a physical inertia to tracked objects, filters out spurious detections and it is implemented as a finite state machine (which is not detailed here for the sake of brevity). The rationale is the following: let us assume that a correct match between the j -th clustered object $o_j(t_{k-1})$ and the i -th bounding box centroid $c_i(t_{k-1})$ is available in the local LIDAR frame $\langle L_{k-1} \rangle$ (this is obtained in $\langle L_0 \rangle$ with an initialisation phase, where the leader stands in front of the robot for about 5 seconds for the initial bootstrap). The robot then moves for δ_t seconds according to the model (1) and updates its position $s(t_k)$ in $\langle L_{k-1} \rangle$ either by using the encoders (if δ_t is sufficiently small) or the global localisation module. After the motion, the information $o_j(t_{k-1})$ and $c_i(t_{k-1})$ are projected in new local frame $\langle L_k \rangle$. Such information form a prior for the next leader detection, and are fused with the new sets of measurements \mathcal{O}_k and $c_i(t_k)$, $\forall i$. Notice that this procedure reduces at the same time the computation times and the probability of mismatch, while making the algorithm robust to lost measurements (either the bounding box or the LIDAR cluster are sufficient for recognition).

C. Global human tracking

Since the human is used as a path-finder for future executions of the path, its position should be estimated in the global reference frame $\langle W \rangle$. To this end, we first need to estimate the robot position $s(t_k)$ in $\langle W \rangle$. This is accomplished fusing together the encoder readings and the LIDAR points $p_i(t_k)$ with an a-priori map of the environment. The $s(t_k)$ robot position and the leader local measurements in $\langle L_k \rangle$ are used to obtain the Cartesian coordinates $(x(t_k), y(t_k))$ of the leader in $\langle W \rangle$.

To track the human being in $\langle W \rangle$, an estimation algorithm is needed, whose main role is to further improve the accuracy of the reconstructed path and to further increase the robustness to occasional sensor failures. The underlying

physical assumption of the leader tracking algorithm is that the leader moves following an unimodal probability density function, i.e., the human cannot move simultaneously in more than one position. In order to limit the computational cost and to comply with the established literature techniques, we assume that this pdf is Gaussian. Thus, two Kalman Filters (KFs) are adopted as tracking filters, whose difference is the adopted motion models. The first one is the constant velocity model, a simplified version of the quite known Social Force Model (SFM) [28]. In this case, a human being is modelled as a point moving with constant velocity. Therefore, being $h(t_k) = [x(t_k), y(t_k), v_x(t_k), v_y(t_k)]^T$ the state at time t_k comprising the position and the velocity of the human on the plane of motion, we have for the corresponding KF

$$\begin{aligned} h(t_{k+1}) &= \begin{bmatrix} 1 & 0 & \delta_t & 0 \\ 0 & 1 & 0 & \delta_t \\ 0 & 0 & 1 & 0 \\ 0 & 0 & 0 & 1 \end{bmatrix} \begin{bmatrix} x(t_k) \\ y(t_k) \\ v_x(t_k) \\ v_y(t_k) \end{bmatrix} + \begin{bmatrix} \frac{\delta_t^2}{2} & 0 \\ 0 & \frac{\delta_t^2}{2} \\ \delta_t & 0 \\ 0 & \delta_t \end{bmatrix} \begin{bmatrix} \nu_x(t_k) \\ \nu_y(t_k) \end{bmatrix} = \\ &= Ah(t_k) + B\nu(t_k), \end{aligned} \quad (3)$$

where $\nu(k)$ is the acceleration noise affecting the velocity variations, supposed to be $\nu(t_k) \sim \mathcal{N}(0, Q)$, with Q being its covariance matrix. The random walk hypothesis is due to the fact that the robot has no knowledge about the actual motion intentions of the human.

The second model instead assumes that humans actually move with a smooth dynamic, as observed in [29]. Hence, the motion model can be approximated by a unicycle dynamic [30]. Hence, we explicitly express the angular and linear velocities as states, and by denoting with $\bar{h}(t_k) = [x(t_k), y(t_k), \theta(t_k), v(t_k), \omega(t_k)]^T$ the state at time t_k (where $\omega(t_k)$ is the angular velocity), we have the following Extended Kalman Filter (EKF) prediction model

$$\begin{aligned} \bar{h}(t_{k+1}) &= \begin{bmatrix} x(t_k) + \delta_t v(t_k) \cos(\theta(t_k)) \\ y(t_k) + \delta_t v(t_k) \sin(\theta(t_k)) \\ \theta(t_k) + \delta_t \omega(t_k) \\ v(t_k) \\ \omega(t_k) \end{bmatrix} + \begin{bmatrix} 0 & 0 \\ 0 & 0 \\ 0 & 0 \\ \delta_t & 0 \\ 0 & \delta_t \end{bmatrix} \begin{bmatrix} \eta_a(t_k) \\ \eta_\omega(t_k) \end{bmatrix} = \\ &= f(\bar{h}(t_k)) + B\eta(t_k), \end{aligned} \quad (4)$$

where $\eta(t_k)$ is the acceleration noise affecting the linear and the angular velocities that is assumed to be $\eta(t_k) \sim \mathcal{N}(0, E)$, with E being its covariance matrix.

The motion models are then selected using the Multiple Model Approach (MMA) presented in [31], which relies on the measurements maximum likelihood approach in a Bayesian setting to estimate the probability in being in one of the two models. However, since humans behave differently in different situations and depending on the context, potential mode changes are considered using the first-order generalised pseudo-Bayesian estimator [31]. This approach fuses together the estimates of each model in a single estimate before the models are adopted, and hence uses the leader measurements

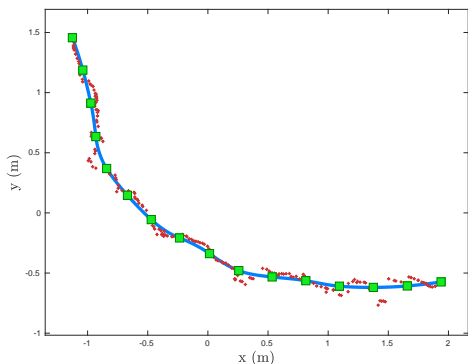


Fig. 5. Example of path fitting and reconstruction. The red stars represent the input data. The green squares are the fitted waypoints, sampled at a uniform distance along the path. The blue solid line is the reconstructed, smoothed path, to be followed by the robot.

to both refine the estimates and the probabilities of each of the two models.

IV. NAVIGATION

The aims of the navigation module are twofold: reconstructing the path followed by the leader in a form that can be followed by the robot, controlling the motion in order for the robot to follow the path with a good accuracy (small deviations are inevitable but they should be kept in check).

A. Path reconstruction

As shown in the scheme in Figure 1, the path reconstruction module continuously receives new information on the current position of the leader from the perception module. This way, it creates a dataset composed of a time series of 2D leader positions which are updated in real-time. The module executes a local path fitting of the estimated leader trajectory. An example execution of the process is shown in Figure 5.

The path is reconstructed using the following steps.

- 1) Once a new leader position is received, it is compared with the previous one, and, if the distance is greater than a small, threshold value, it is recorded into the dataset. This action is necessary to handle the scenario where the leader stops for a long time, in order to avoid an unnecessary growth of the dataset.
- 2) When the new position qualifies for its inclusion into the dataset, the x and y components of the datapoints are fitted using a classical smoothing algorithm, i.e. the LOESS (Locally Estimated Scatterplot Smoothing) [32].
- 3) The fitted datapoints are then connected by a polyline, and a number of waypoints are sampled at a uniform curvilinear distance (corresponding to the green squares of Figure 5).
- 4) The waypoints are connected by a G2 clothoid spline (corresponding to the solid blue line of Figure 5), using the algorithms and techniques discussed in [33], [34], and for which an efficient C++ implementation is available [35].

The choice of the clothoid comes from the observation that humans tend to follow a unicycle-like dynamics [30] given in (4), which naturally generates clothoid curves. What is more, clothoids have been proved to be effective to mimic a human path by a robotic agent [36], for the continuity of the curves and of their curvature.

B. Robot control

When a path is reconstructed, following the steps described above, the controller module takes the responsibility to execute a safe navigation of the robot following as closely as possible the prescribed path. For this work, we employed the path following algorithm described in [37], which is velocity-independent and avoids the singularities presented by other common algorithms when the vehicle has to stop and the velocity is set to zero. The velocity of the robot is chosen by our controller based both on the distance from the end of the path (corresponding to the leader position), with the aim of following the leader at a constant (curvilinear) distance, on the current path curvature (the vehicle is slowed down when traveling a sharp curve), and on the past robot velocities (to limit the maximum allowed accelerations).

In addition to following the path, the control module implements a safety policy whereby when an obstacle is encountered along the path the robot first slows down, and then stops if the occlusion does not pass away. During this phase, if the distance from the leader becomes too large, the robot emits a sound signal to notify the exception and to attract the leader's attention.

V. EXPERIMENTAL RESULTS

A first set of experiments were to decide the most effective combination of solutions for vision-based detection and recognition. As regards detection, our evaluation lead to the adoption of SSD, since it implements the CNN with a relatively small number of parameters. The result is a low computation time, which comes at the price of a slight detection inaccuracy, which is however compensated by the fusion module. The recognition module based on KNN has been tested on the Market1501 dataset [27]: by comparing the results obtained by the KNN in combination with ResNet50 (which produced approximately 50% of correct responses) and GoogLeNet (more than 90% of correct responses), the latter emerged as an obvious choice. Finally, for the image tracker, our aim is to process long real-time sequence with occasional total occlusions and changes of shape. We evaluated the computation performance of each of the methods presented in Section II. The results, which are reported in Table I frame-per-second, suggested us the adoption of KCF, CSRT and MOSSE.

A. Performance evaluation of the system as a whole

The algorithms presented in Section III and Section IV were executed on a Jetson TX2³ for the acquisition of the RGB-D

³<https://www.nvidia.com/en-us/autonomous-machines/embedded-systems/jetson-tx2/>

TABLE I

OVERVIEW OF THE FPS RATE OF THE IMAGE TRACKING ALGORITHMS. THE PERFORMANCES WERE MEASURED ON AN INTEL CORE I5 CPU AND ON AN NVIDIA JETSON TX2 GPU.

	MIL	KCF	MedFlow	CSRT	MOSSE	GOTURN	TLD
FPS	9	38	40	15	56	20	10

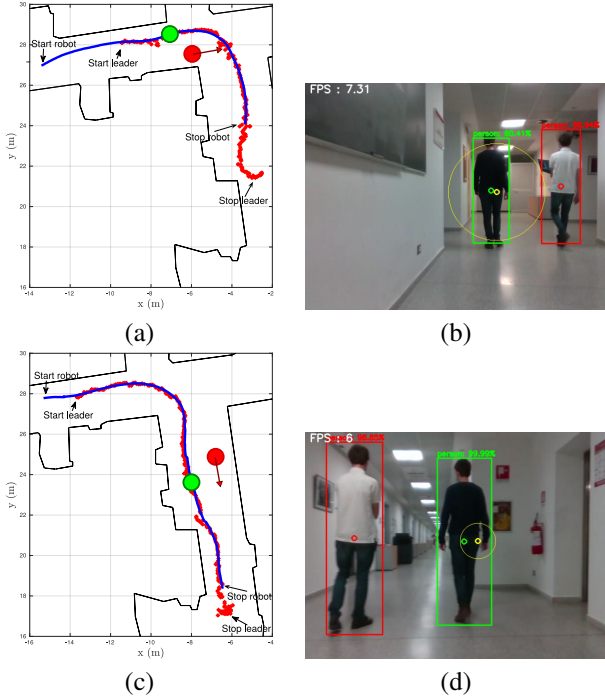


Fig. 6. Experimental trajectories in a hallway. The leader and a pedestrian walk in the same corridor with (a,b) partially occluding trajectories and (c,d) missing and recovering of the leader with the camera tracking. (a,c) depict the trajectory followed by the robot (solid blue line) and the measured leader positions (red stars), while the green and red circles correspond to the positions of the leader and the other pedestrian, respectively, when the camera snapshots shown in (b,d) are grabbed.

data and the classifier, while the LIDAR scans, the sensing data fusion, and the navigation control were executed on a NUC, both on board of the wheeled robot entirely assembled at the University of Trento. Further experiments were carried out in our department at the University of Trento. First, we present the performance and robustness of the leader tracking algorithm. To this end, we record the data in two different portions of an hallway of our department with multiple exits and in different circumstances. In Figure 6-b, the robot follows the leader while another pedestrian is walking nearby, however the tracking is correctly maintained on the leader (see Figure 6-a for the trajectories). Similar results are obtained for crossing trajectories or when the leader exits from the camera field of view for the right turn but the other pedestrian is not wrongly classified as the leader, which is tracked back after the turn (Figure 6-c,d).

For a qualitative analysis of the tracking and navigation, we present in Figure 7 an example of the comparison of the robot trajectory (blue line) with the actual position of the leader (red

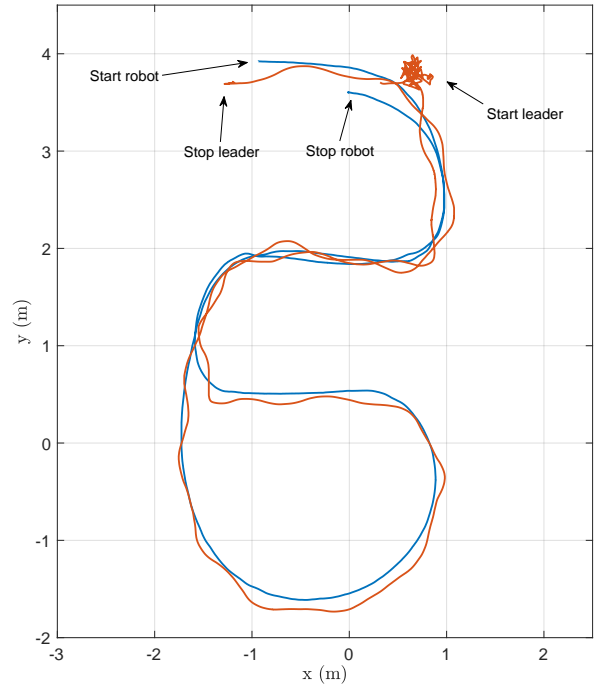


Fig. 7. An example of the actual leader path (red line) and robot trajectory (blue line).

line), both captured with a network of eight OptiTrack cameras for ground truth reference. Notice the leader starting position standing in front of the robot during the bootstrap phase. The swinging leader trajectory is dictated by the OptiTrack tracked markers placed on the head of the human to avoid occlusions, hence oscillating with the footsteps. From this picture it is evident that, in sharp turns, the robot loses the image tracking of the leader, but it is nonetheless able to exactly follow his path by means of the fusion with the LIDAR data. Finally, we would like to point out that the error in the trajectory followed by the robot with respect to the human footsteps is in the range of ± 25 cm, i.e. the typical encumbrance of the human body.

Due to stringent space limitations, further experimental evidences of the effectiveness of the approach can be found in the video accompanying this paper.

VI. CONCLUSIONS AND FUTURE WORK

In this paper, we have presented an approach for guiding a robot across a difficult environment. A human operator takes the role of a path-finder and the robot follows, moving in a close neighbourhood of the path physically marked by the human with her/his footsteps. This application required a combination of state-of-the-art techniques for robust perception and path reconstruction. The experimental results show the high level of reliability and robustness reached by the proposed solution.

Different points remain open and are reserved for future work. A first work direction is releasing the assumption that the robot is in possession of a map and can rely on a global localisation system. We envisage a scenario in which

the map is constructed while the robot follows its leader and it only relies on a relative localisation with respect to reference points identified in the environment and to its leader. Another important direction is a theoretical study of how the interaction between model based approaches and neural networks can produce results with a guaranteed accuracy. Finally, a possibility we are considering is the use of wearable haptic bracelets and the implementation of a protocol that the robot can use to notify to its leader the occurrence of exceptional conditions (e.g., when the path is too close to an obstacle and the robot cannot follow it within appropriate safety margins).

REFERENCES

- [1] M. J. Islam, J. Hong, and J. Sattar, "Person-following by autonomous robots: A categorical overview," *The International Journal of Robotics Research*, vol. 38, no. 14, pp. 1581–1618, 2019.
- [2] S. Jiang, J. Zhang, Y. Zhang, F. Qiu, D. Wang, and X. Liu, "Long-term tracking algorithm with the combination of multi-feature fusion and yolo," in *Chinese Conference on Image and Graphics Technologies*. Springer, 2018, pp. 390–402.
- [3] W. Liu, D. Anguelov, D. Erhan, C. Szegedy, S. Reed, C.-Y. Fu, and A. C. Berg, "Ssd: Single shot multibox detector," in *European conference on computer vision*. Springer, 2016, pp. 21–37.
- [4] J. Redmon, S. Divvala, R. Girshick, and A. Farhadi, "You only look once: Unified, real-time object detection," in *Proceedings of the IEEE conference on computer vision and pattern recognition*, 2016, pp. 779–788.
- [5] R. Girshick, J. Donahue, T. Darrell, and J. Malik, "Rich feature hierarchies for accurate object detection and semantic segmentation," in *Proceedings of the IEEE conference on computer vision and pattern recognition*, 2014, pp. 580–587.
- [6] Z. Cao, G. Hidalgo, T. Simon, S.-E. Wei, and Y. Sheikh, "Openpose: realtime multi-person 2d pose estimation using part affinity fields," *IEEE transactions on pattern analysis and machine intelligence*, vol. 43, no. 1, pp. 172–186, 2019.
- [7] A. Neubeck and L. Van Gool, "Efficient non-maximum suppression," in *18th International Conference on Pattern Recognition (ICPR'06)*, vol. 3. IEEE, 2006, pp. 850–855.
- [8] M. A. Hearst, S. T. Dumais, E. Osuna, J. Platt, and B. Scholkopf, "Support vector machines," *IEEE Intelligent Systems and their applications*, vol. 13, no. 4, pp. 18–28, 1998.
- [9] C.-M. Pun, X.-C. Yuan, and X.-L. Bi, "Image forgery detection using adaptive oversegmentation and feature point matching," *IEEE Transactions on Information Forensics and Security*, vol. 10, no. 8, pp. 1705–1716, 2015.
- [10] P. M. Roth, M. Hirzer, M. Köstinger, C. Belezni, and H. Bischof, "Mahalanobis Distance Learning for Person Re-Identification," in *Person Re-Identification*, ser. *Advances in Computer Vision and Pattern Recognition*, S. Gong, M. Cristani, S. Yan, and C. C. Loy, Eds. London, United Kingdom: Springer, 2014, pp. 247–267.
- [11] E. Ristani and C. Tomasi, "Features for multi-target multi-camera tracking and re-identification," in *Proceedings of the IEEE conference on computer vision and pattern recognition*, 2018, pp. 6036–6046.
- [12] C. Szegedy, W. Liu, Y. Jia, P. Sermanet, S. Reed, D. Anguelov, D. Erhan, V. Vanhoucke, and A. Rabinovich, "Going deeper with convolutions," in *Proceedings of the IEEE conference on computer vision and pattern recognition*, 2015, pp. 1–9.
- [13] K. He, X. Zhang, S. Ren, and J. Sun, "Identity mappings in deep residual networks," in *European conference on computer vision*. Springer, 2016, pp. 630–645.
- [14] B. Babenko, M.-H. Yang, and S. Belongie, "Robust object tracking with online multiple instance learning," *IEEE transactions on pattern analysis and machine intelligence*, vol. 33, no. 8, pp. 1619–1632, 2010.
- [15] J. F. Henriques, R. Caseiro, P. Martins, and J. Batista, "Exploiting the circulant structure of tracking-by-detection with kernels," in *European conference on computer vision*. Springer, 2012, pp. 702–715.
- [16] Z. Kalal, K. Mikolajczyk, and J. Matas, "Forward-backward error: Automatic detection of tracking failures," in *2010 20th international conference on pattern recognition*. IEEE, 2010, pp. 2756–2759.
- [17] A. Lukezic, T. Vojir, L. Čehovin Zajc, J. Matas, and M. Kristan, "Discriminative correlation filter with channel and spatial reliability," in *Proceedings of the IEEE conference on computer vision and pattern recognition*, 2017, pp. 6309–6318.
- [18] D. S. Bolme, J. R. Beveridge, B. A. Draper, and Y. M. Lui, "Visual object tracking using adaptive correlation filters," in *2010 IEEE computer society conference on computer vision and pattern recognition*. IEEE, 2010, pp. 2544–2550.
- [19] D. Held, S. Thrun, and S. Savarese, "Learning to track at 100 fps with deep regression networks," in *European conference on computer vision*. Springer, 2016, pp. 749–765.
- [20] Z. Kalal, K. Mikolajczyk, and J. Matas, "Tracking-learning-detection," *IEEE transactions on pattern analysis and machine intelligence*, vol. 34, no. 7, pp. 1409–1422, 2011.
- [21] A. Antonucci, V. Magnago, L. Palopoli, and D. Fontanelli, "Performance assessment of a people tracker for social robots," in *2019 IEEE International Instrumentation and Measurement Technology Conference (I2MTC)*. IEEE, 2019, pp. 1–6.
- [22] W. Zhen, Y. Hu, J. Liu, and S. Scherer, "A joint optimization approach of lidar-camera fusion for accurate dense 3-d reconstructions," *IEEE Robotics and Automation Letters*, vol. 4, no. 4, pp. 3585–3592, 2019.
- [23] R. W. Wolcott and R. M. Eustice, "Visual localization within lidar maps for automated urban driving," in *2014 IEEE/RSJ International Conference on Intelligent Robots and Systems*. IEEE, 2014, pp. 176–183.
- [24] S. Hwang, N. Kim, Y. Choi, S. Lee, and I. S. Kweon, "Fast multiple objects detection and tracking fusing color camera and 3d lidar for intelligent vehicles," in *2016 13th International Conference on Ubiquitous Robots and Ambient Intelligence (URAI)*. IEEE, 2016, pp. 234–239.
- [25] J. Redmon and A. Farhadi, "Yolov3: An incremental improvement," *arXiv preprint arXiv:1804.02767*, 2018.
- [26] A. G. Howard, M. Zhu, B. Chen, D. Kalenichenko, W. Wang, T. Weyand, M. Andreetto, and H. Adam, "Mobilenets: Efficient convolutional neural networks for mobile vision applications," *arXiv preprint arXiv:1704.04861*, 2017.
- [27] L. Zheng, L. Shen, L. Tian, S. Wang, J. Wang, and Q. Tian, "Scalable person re-identification: A benchmark," in *Proceedings of the IEEE international conference on computer vision*, 2015, pp. 1116–1124.
- [28] D. Helbing and P. Molnar, "Social force model for pedestrian dynamics," *Physical review E*, vol. 51, no. 5, p. 4282, 1995.
- [29] G. Arechavalaeta, J.-P. Laumond, H. Hicheur, and A. Berthoz, "On the nonholonomic nature of human locomotion," *Autonomous Robots*, vol. 25, no. 1, pp. 25–35, 2008.
- [30] F. Farina, D. Fontanelli, A. Garulli, A. Giannitrapani, and D. Praticchizzo, "Walking ahead: The headed social force model," *PLoS one*, vol. 12, no. 1, p. e0169734, 2017.
- [31] T. K. Y. Bar-Shalom, X. Rong Li, *Estimation with Application to Tracking and Navigation – Theory, Algorithm and Software*. John Wiley and Sons, 2001.
- [32] W. S. Cleveland, "Robust locally weighted regression and smoothing scatterplots," *Journal of the American statistical association*, vol. 74, no. 368, pp. 829–836, 1979.
- [33] E. Bertolazzi and M. Frego, "On the G2 Hermite interpolation problem with clothoids," *Journal of Computational and Applied Mathematics*, vol. 341, pp. 99–116, 2018.
- [34] —, "Interpolating clothoid splines with curvature continuity," *Mathematical Methods in the Applied Sciences*, vol. 41, no. 4, pp. 1723–1737, 2018.
- [35] E. Bertolazzi, P. Bevilacqua, and M. Frego, "Clothoids: a C++ library with Matlab interface for the handling of clothoid curves," *Rend. Sem. Mat. Univ. Pol. Torino*, vol. 76, no. 2, pp. 47–56, 2018.
- [36] P. Bevilacqua, M. Frego, D. Fontanelli, and L. Palopoli, "Reactive Planning for Assistive Robots," *IEEE Robotics and Automation Letters*, vol. 3, no. 2, pp. 1276–1283, April 2018.
- [37] M. Andreetto, S. Divan, D. Fontanelli, and L. Palopoli, "Harnessing steering singularities in passive path following for robotic walkers," in *2017 IEEE International Conference on Robotics and Automation (ICRA)*. IEEE, 2017, pp. 2426–2432.